Propagation of an idealized infection in an airway tree, consequences of the inflammation on the oxygen transfer to blood

Frédérique Noël, Benjamin Mauroy

Propagation of an idealized infection in an airway tree, consequences of the inflammation on the oxygen transfer to blood

Frédérique Noël[1,*] and Benjamin Mauroy[2,†]

[1] *COMMEDIA, Inria Paris, Paris, France*
[2] *Université Côte d'Azur, CNRS, LJAD, Vader center, Nice, France*

(Dated: January 6, 2023)

A mathematical model of infection, inflammation and immune response in an idealized bronchial tree is developed. This work is based on a model from the literature that is extended to account for the propagation dynamics of an infection between the airways. The inflammation affects the size of the airways, the air flows distribution in the airway tree, and, consequently, the oxygen transfers to blood. We test different infections outcomes and propagation speed. In the hypotheses of our model, the inflammation can reduce notably and sometimes drastically the oxygen flow to blood. Our model predicts how the air flows and oxygen exchanges reorganize in the tree during an infection. Our results highlight the links between the localization of the infection and the amplitude of the loss of oxygen flow to blood. We show that a compensation phenomena due to the reorganization of the flow exists, but that it remains marginal unless the power produced the ventilation muscles is increased. Our model forms a first step towards a better understanding of the dynamics of bronchial infections.

Declarations of interest: none.

Keywords: Lung, pulmonary infection, inflammation, airways, air fluid mechanics, oxygen transport, oxygen transfer to blood, mathematical model, numerics

INTRODUCTION

The lung is a complex system that serves as an exchange interface between the ambient air and blood [1]. It transports the oxygen present in the ambient air through its tree-like structure to blood and removes carbon dioxide from it. However, because of its direct interface with the external environment, the lung is prone to develop infections [2] that can affect its ventilation [3]. Lung infections, such as pneumonia, are highly prevalent in the population and more specifically in populations with lung transplants, cystic fibrosis, COPD, etc. [4–7]. Recently the coronavirus SARS-CoV-2 (COVID-19) has appeared in China and has spread to become a global pandemic [8]. This virus, which has acute lung injury and acute respiratory distress as major symptoms [9], has affected at this date about 300 millions of people and has killed about 5 millions of people, with these numbers still rising [10].

The lung forms a humid environment, full of oxygen, and is connected to the ambient air through mouth and nose. Hence, for pathogens, this organ is easy to infiltrate and a good medium for proliferation. To counteract this potential threat, the lung has developed mechanical protections against infections. The mechanical protection is based on the existence of the bronchial mucus that covers the airways wall [11]. The bronchial mucus acts as a barrier against infections by capturing the pathogens. The mucus is motioned towards the upper respiratory system by cough [12] and mucociliary clearance, i.e. pushed by cilia localized on the airway walls [13]. Once in the oesopharyngeal pathway, mucus is eliminated, either by being swallowed or expelled by cough. These mechanisms can be dysfunctional [14] (pathology, lack of maturity in children, aging) and not efficient enough to avoid the development of a pathogen. They are completed by the immune system that is able to fight infections occurring in the lung [15]. The development of an infection induces an inflammation in bronchi. This reaction makes the tissue to swell in order for the white blood cells of the immune system to converge at the site of infection and to start eliminating the pathogens [15]. The inflammation modifies the geometry of the lung, and hence the distribution of the airflow and the ventilation.

Different approaches in the literature have been used to model the response of the immune system following a pulmonary infection. A first approach is to model the macrophage response after an infection using ordinary differential equations [16] or using models of granulomas development [17–19], which are macrophage clusters. These types of approaches have the benefit of mimicking the immune response specific to the lung and allows to explore potential treatments. However, even if macrophages are the first responders during a pulmonary infection, these models do not take into account neutrophils present in the blood that are the majority of the leucocytes. A second approach has been to model the inflammatory response in a part of an acinus [20]. This model allows to represent the infection in the whole lung and to model the exchanges with blood. However, even if this model takes into consideration the swelling of tissue, it does not represent the pathogen evolution in the lung,

* frederique.noel@inria.fr
† benjamin.mauroy@univ-cotedazur.fr

which is important in order to be able to model different types and speeds of infection.

In this paper, we use a more global immune response model that is not specific to the lung and that can be used in any organs. This type of models has the benefit of not being specific to a single virus or bacteria. Nevertheless, simple models with only three [21–23] or four different variables [24–27] describe the evolution of tissue damage all along the infection, but not the tissue inflammation. Hence, we used a more specific, but also more complex model [28] that describes not only the immune response in the tissue and blood, but also the tissue inflammation. This last model is then linked to the gas transport model introduced in [29, 30] to simulate the propagation of an infection in an idealized lung and to simulate inflammation bronchi per bronchi. Our model is generic, it does not focus on one pathogen only. In this explorative model, we study different stages of the infection and how the exchanges with blood are affected by the altered lung's geometry arising from the inflammation of its airways.

In the following section, we start by introducing a model of the response to a pathogen of the innate biological immune system. Then, we describe a model of an infection propagation and of the resulting modification on the transport of respiratory gases in the lung. In the next section, we analyse our simulations for three different outcomes: cured, aseptic death and septic death. The model predicts that, depending on the localization of the infection in the lung and its stage, the lung's ventilation might become very costly in term of energy, up to a point where it is not able to sustain anymore the body needs in oxygen.

MODELLING

The value of the parameters of the model describe in the next sections and of the numerical simulations are given in Table I in Appendix A.

Model of the human lung

Non inflamed lung. The model of the human lung used in this work is the same as in [29–31]. The model is based on the assembly of self-similar trees that mimic the functional regions of the lung. Self-similar trees have been thoroughly used in the literature to model the mammalian lungs and have allowed to uncover many interesting behaviors of the lung [29–34]. The lung is modelled as a tree of bifurcating cylindrical airways. Each airway has a generation index that corresponds to the number of bifurcations from the airway up to the root of the tree, which mimics the trachea. The tree consists in 23 successive generations of cylinders [1], numbered from 0 to $N = 22$. The root of the tree that mimics the trachea has a length l_0 and a radius $r_{0,\mathrm{he}}$. The airways from the last generation are referred to as the terminal airways. The conductive tree is modelled with the $G = 17$ first bifurcations (represented in orange in Figure 1) [1], whose generation indexes are ranging from 0 to $G-1$. In the conductive tree, the respiratory gas are only conveyed and no exchange with blood occurs. The size of the airways in our model of the conductive tree is decreasing at each bifurcation with a ratio $h = \left(\frac{1}{2}\right)^{\frac{1}{3}}$ [1, 32]. Hence, the radii $r_{i,\mathrm{he}}$ and length l_i of an airway in the generations $i \in [\![0, G-1]\!]$ are

$$r_{i,\mathrm{he}} = r_{0,\mathrm{he}} h^i \quad \text{and} \quad l_i = l_0 h^i$$

The acini, where the respiratory gas exchange occurs, are modelled by the $H = 6$ last generations of our tree (represented in blue in Figure 1) [1]. The airways in the tree that mimics the acini are called the respiratory airways. In our model, all the airways in the acini have the same size [1]. As a consequence, the radii $r_{i,\mathrm{he}}$ and length l_i of the airways in the model of the acini are

$$r_{i,\mathrm{he}} = r_{0,\mathrm{he}} h^{G-1} \quad \text{and} \quad l_i = l_0 h^{G-1}$$

for generations $i \in [\![G, N]\!]$. To mimic the exchange surface with blood in the acini, the airways in our model of acini are layered with "virtual" alveoli represented by the exchange surface area per unit of airway wall surface area, ρ_s [30].

Inflamed lung geometry. In the tree that mimics the non inflamed lung, the bifurcations are symmetric, i.e. an airway divides into two identical airways. Nevertheless, when an inflammation develops in an airway, it will decrease its radius and break the symmetry of the bifurcation from which it originates. Hence, air and respiratory gas will go through a tree potentially with asymmetric bifurcations. To the contrary of the model in [30], where airways could be studied only through their generation index, here, each airway of the tree could have its own behavior. Consequently, the airways have to be indexed independently. An airway is localized in the tree using its generation index $i \in [\![0, N]\!]$ and its position j in the generation i with $j \in [\![0, 2^i - 1]\!]$. The root of the tree index is $(0, 0)$. The two branches originating from the bifurcation of an airway indexed (i, j) are indexed by $(i+1, 2j)$ and $(i+1, 2j+1)$, as schematized in Figure 1.

The inflamed radii are denoted $r_{i,j}$ and the corresponding surface area of the airway cross section is $S_{i,j} = \pi r_{i,j}^2$.

Depending on the locations of the inflamed airways, the physical and geometrical properties of several paths from the root of the tree to the terminal airways are identical. Hence, we regroup these paths into sets called *path types*, see an example in Figure 6A. The physical analysis can then be performed only once per path type.

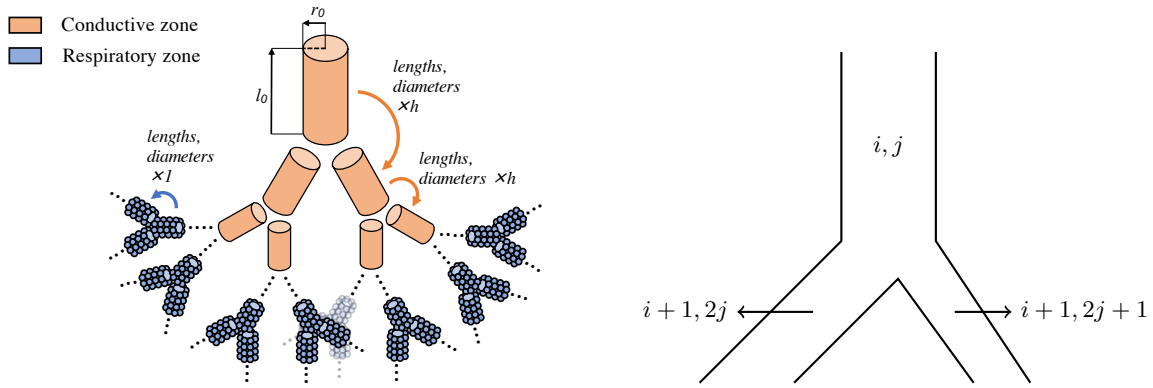

FIG. 1. **Left:** The non inflamed lung is modelled as a tree of bifurcating cylindrical airways. Each airway has a generation index that corresponds to the number of bifurcations from the airway up to the root of the tree, which mimics the trachea. The tree consists in 23 successive generations of cylinders. The root of the tree that mimics the trachea has a length l_0 and a radius r_0. The conductive tree is modelled with the 17th first bifurcations (beige). In the conductive tree, the respiratory gas are only conveyed and no exchange with blood occurs. The size of the airways in our model of the conductive tree is decreasing at each bifurcation with a ratio $h = \left(\frac{1}{2}\right)^{\frac{1}{3}}$. The acini, where the respiratory gaz exchange occurs, are modelled by the 6 last generations of our tree (blue). All the airways in the acini have the same size. **Right:** The inflammation can break the symmetry of the bifurcations in our model. Hence, each airway of our model has to be indexed independently to the others. Indices of the bronchi in an asymmetric bifurcation. The root of the tree that mimics the trachea is indexed $(0, 0)$. An airway with index (i, j) bifurcates into two airways with indices $(i + 1, 2j)$ and $(i + 1, 2j + 1)$.

This approach reduces drastically the model computational cost when the inflammation is limited to a subpart of the tree. However, when the inflammation reaches a large number of airways, the number of path types increases, eventually becoming close to the number of terminal airways. If the number of path types becomes very large, then the path types strategy becomes equivalent in term of computational cost to the straightforward strategy of analyzing independently the physics of each airways of the tree. In this work, we focus on upper respiratory tract infections, such as common cold, influenza or acute bronchitis, that reach the large airways of the lung only [35, 36]. Large airways correspond to airways with a diameter larger than 2-3 mm [37], i.e. down to the nine first generations of our model of the bronchial tree. Mimicking such infections using the path types strategy allows to keep the computational cost low.

Fluid mechanics in the airways. We assume that the pressure drop $\Delta p_{i,j}$ in the airway (i, j) is proportional to the airflow $q_{i,j}$ in the airway,

$$\Delta p_{i,j} = R_{i,j} q_{i,j}$$

The quantity $R_{i,j}$ is the hydrodynamic resistance of the airway, it depends on the airway geometry and on the regime of the airflow [38–40]. In this work, we assume that the air flows according to the Poiseuille regime, i.e. we assume that the air flow in the airways is low and developed. Hence, the hydrodynamic resistance of the airway (i, j) expresses as $R_{i,j} = \frac{8\mu l_i}{\pi r_{i,j}^4}$ [32], where μ is the viscosity of the air. This hypothesis corresponds to a first level of approximation of the air fluid dynamics. It allows to keep the model more tractable and to isolate the influence on the model predictions of each of the process included in the model. The air inertia, known to exist in the large airways [41], should be included in a future study as an improvement of the model.

In asymmetrical bifurcations, the airflow is conserved but does not divide equally. In the airway (i, j), the airflow $q_{i,j}$ splits between the two airways $(i+1, 2j)$ and $(i + 1, 2j + 1)$,

$$q_{i,j} = q_{i+1,2j} + q_{i+1,2j+1}.$$

In order to compute the distribution of the airflows in the whole tree, we assume that the same mechanical pressure is applied everywhere in the lung by the ventilation [42–44]. As a consequence, the airflows in a bifurcation verify [44]:

$$q_{i+1,2j} = q_{i,j} \frac{R^{\text{eq}}_{i+1,2j+1}}{R^{\text{eq}}_{i+1,2j} + R^{\text{eq}}_{i+1,2j+1}}$$
$$q_{i+1,2j+1} = q_{i,j} \frac{R^{\text{eq}}_{i+1,2j}}{R^{\text{eq}}_{i+1,2j} + R^{\text{eq}}_{i+1,2j+1}}$$

where $R^{\text{eq}}_{k,l}$ is the equivalent resistance of the subtree spanning from the airway (k, l). If the subtrees spanning from the airways $(i + 1, 2j)$ and $(i + 1, 2j + 1)$ are identical, then $R^{\text{eq}}_{i+1,2j} = R^{\text{eq}}_{i+1,2j+1}$ and the airflow splits equally: $q_{i+1,2j} = q_{i+1,2j+1} = \frac{q_{i,j}}{2}$ as in [29]. In the airway (i, j), the air flows along the axis of the airway with a mean velocity of $u_{i,j} = q_{i,j}/S_{i,j}$.

Ventilation amplitude. When the lung is inflamed, the airways geometry is affected and the ventilation is modified. In the following, we assume that the air pressure drop Δp between the root of the tree and the deeper airways is fixed. This hypothesis means that the energy spent by the patient for ventilating the lung is the same before, during and after the infection. The energy brought to air is proportional to the pressure drop applied to the tree. Due to energy conservation, this energy is split into kinetic energy (air motion) and dissipated viscous energy (heat) [45]. When the hydrodynamic resistance increases, then for the same amount of energy put in the system, more heat is produced and the motion of air is reduced.

The air pressure drop Δp throughout the whole tree depends on the total air flow rate $q_{0,0}$ through the tree and on the hydrodynamic resistance R of the airway tree [44],

$$\Delta p = R q_{0,0} = R S_{0,0} u_{0,0} \tag{1}$$

In our model, the resistance of the healthy case R_{He} is computed directly from the Poiseuille resistance of the airways [32]. In the inflamed case, we have to account for the effect of the occlusion of several airways on the resistance. The hydrodynamic resistance of the lung is complex and affected by many phenomena, hence it is difficult to get a correct estimation in an idealized model such as ours. Typically, our model does not include detailed bifurcations geometries or inertial effects, which are known to affect the resistance [40]. Nevertheless, the equivalent idealized hydrodynamic resistance computed in our model accounts for the influence of the airways radii and is able to determine realistic trends in term of resistance variation. Hence, when the airway radii are affected by inflammation, we compute the relative change λ of the idealized resistance. Then, we apply this same relative change to the healthy hydrodynamic resistance from in the literature and $R = \lambda R_{\mathrm{he}}$.

The idealized hydrodynamic resistance of the tree can be computed by recurrence. The airway of the first generation of the tree, which mimics the trachea, divides into two subtrees T_1 and T_2 which have each their own resistance, say R_1 and R_2. The equivalent resistance R of the tree is then, $R = R_{0,0} + \left(\frac{1}{R_1} + \frac{1}{R_2}\right)^{-1}$. The resistance of the two subtrees T_1 and T_2 is computed in the same way.

The velocity of the air in the root of the tree is

$$u_{0,0}(t) = A \sin\left(\frac{2\pi}{T} t\right)$$

where A is the amplitude of the ventilation and T its period.

The pressure drop between the inlet and the outlet of the tree and the period of ventilation are assumed to remain the same before, during and after the inflammation, $\Delta P_{\mathrm{he}}(t) = \Delta P(t)$. Using the equation (1), we can then deduce that the ventilation amplitude for an inflammation that affects the airways diameters and the hydrodynamic resistance of the tree is

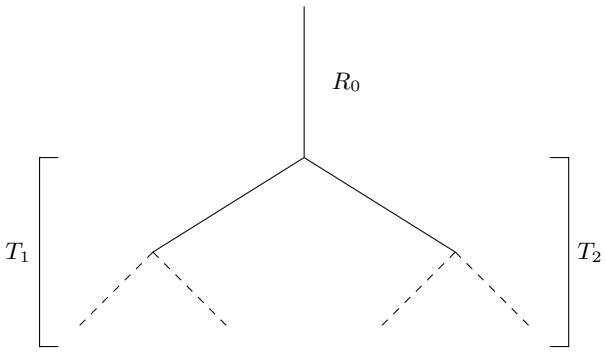

FIG. 2. Computation by recurrence of the equivalent resistance of the airway tree. The subtrees T_1 and T_2 have a resistance of R_1 and R_2 respectively. The total equivalent resistance of the tree is then $R = R_0 + \left(\frac{1}{R_1} + \frac{1}{R_2}\right)^{-1}$. The resistance of the subtree T_1 and T_2 are then computed in the same way. We go on until we reach the end of the tree.

$$A = A_{\mathrm{he}} \frac{R_{\mathrm{he}}}{R} \frac{r_{0,\mathrm{he}}^2}{r_{0,0}^2} \tag{2}$$

Gas transport model in a tree with asymmetric bifurcations

In [29], we modelled the transport of oxygen and carbon dioxide in an idealized dichotomic tree with symmetric bifurcations. However, when inflammation appears in a bronchus, its air lumen is modified. We will consider in our model that the change in lumen area is related to an alteration of the airway radius only. This implies that the bifurcation from which an inflamed airway originates is no longer symmetric, as schematized in Figure 1. Hence, the model of oxygen transport in the lung from [29] has to be extended to account for asymmetric bifurcations.

Transport equation. The transport of oxygen and carbon dioxide in the lung is driven by three phenomena: convection by the airflow, diffusion and exchange with blood through the alveoli walls in the respiratory airways.

Due to the decrease of the air velocity along the airway generations, oxygen is mainly transported by convection in the proximal (large) airways, while oxygen is mainly transported by diffusion in the distal (small) airways [1].

Because we assume Poiseuille regime in the airways, the air velocity is oriented along the airway axis with a parabolic profile on the airway section. The velocity is maximal on the axis of the airway and zero on its wall. If we consider at first the convective transport of oxygen

only, this non homogeneous air velocity profile would induce a non homogeneous oxygen distribution on the airway section. This inhomogeneity would appear in the form of a layer at the airway wall. It would correspond to the region of the airway where the air velocity is low enough so that convection has not enough time to bring oxygen there. However, this inhomogeneity would correspond to a radial oxygen concentration gradient. Hence, radial diffusion would occur, moving oxygen from the core of the airway toward the layer. This diffusion process would be performed with a characteristic velocity of the order of $D/h_{i,j}$, where $D \simeq 0.2\ 10^{-4}\ \mathrm{m}^2.\mathrm{s}^{-1}$ is the diffusion coefficient of oxygen in air and $h_{i,j}$ would be the characteristic thickness of the layer. The characteristic thickness $h_{i,j}$ is difficult to evaluate without a full 3D simulation, but we know that it would be much smaller than the airway radius $r_{i,j}$. As a consequence, the radial diffusion velocity would be much larger than 2 $\mathrm{mm.s}^{-1}$ in the trachea (radius of about 1 cm) and than 8 $\mathrm{mm.s}^{-1}$ in the respiratory bronchioles (radius of about 0.25 mm). Thus, neglecting in our model the variation of the oxygen distribution on the section of the airways is a good first approximation.

Our model is based on computing the mean partial pressure of the gas over the section of an airway. This pressure is transported along the longitudinal axis x of the airway. With these modeling hypotheses, the system of equations mimicking the transport consists in the superposition of $2^{N+1}-1$ unidimensional equations, one per airway, coupled together through the bifurcations. Hence, the partial pressure $P_{i,j}(x,t)$ of the respiratory gas in an airway (i,j) follows the convection–diffusion–reaction equation

$$\frac{\partial P_{i,j}}{\partial t} - D\frac{\partial^2 P_{i,j}}{\partial x^2} + u_{i,j}(t)\frac{\partial P_{i,j}}{\partial x} + \beta_{i,j}P_{i,j} = \beta_{i,j}P_{\mathrm{blood}}(P_{i,j}), \tag{3}$$

for $x \in [0, l_i]$, where l_i is the length of an airway in generation i. The quantity D is the diffusion coefficient of the gas in the air, $u_{i,j}(t)$ is the velocity of the air in the bronchus j of generation i. The function $P_{\mathrm{blood}}(P_{i,j})$ is the partial pressure of the gas in blood assuming the equality of the oxygen flow through the membrane and the oxygen flow carried away by blood, see Appendix B and [29, 30, 46]. The quantity $\beta_{i,j}$ is a coefficient reflecting the exchange of the gas between the airways and the blood. The exchange coefficient depends on the generation of the airway. Indeed, in the conductive airways (for $i \in [\![0, G-1]\!]$), there is no gas exchange between airways and blood, whereas in the respiratory airways (for $i \in [\![G, N]\!]$), the gas exchange occurs through the wall of the airways. The exchange coefficient is then defined as dependent on the generation index:

$$\beta_i = \begin{cases} 0, & \text{for } i \in [\![0, G-1]\!] \\ \rho_s \dfrac{2k}{r_A}\alpha_i & \text{for } i \in [\![G, N]\!] \end{cases} \tag{4}$$

where k is the ratio relating partial pressure of the gas to its concentration in water, r_A is the radius of the respiratory airways and α_i is the alveolocapillary membrane permeability defined by [46]

$$\alpha_i = \begin{cases} 0, & \text{for } i \in [\![0, G-1]\!], \\ \alpha = \dfrac{D_{\mathrm{O_2,H_2O}}\ \sigma_{\mathrm{O_2,H_2O}}}{\tau}, & \text{for } i \in [\![G, N]\!] \end{cases} \tag{5}$$

where $D_{\mathrm{O_2,H_2O}}$ is the diffusion coefficient of the gas in water, $\sigma_{\mathrm{O_2,H_2O}}$ is the solubility coefficient of the gas in water and τ is the thickness of the alveolar membrane.

Conditions at the bifurcation. The bifurcations are not accounted for geometrically but by using a set of equations representing mass conservation and pressure continuity. By affecting the radius of several airways, the inflammation makes some bifurcations asymmetric. These asymmetric bifurcations affect the air flow distribution in the tree and, hence, the gas flow distribution. The gas flow is conserved through a bifurcation,

$$\begin{aligned} S_{i,j}\left(-D\frac{\partial P_{i,j}(l_{i,j},t)}{\partial x} + u_{i,j}(t)P_{i,j}(l_{i,j},t)\right) = \\ S_{i+1,2j}\left(-D\frac{\partial P_{i+1,2j}(0,t)}{\partial x} + u_{i+1,2j}(t)P_{i+1,2j}(0,t)\right) + \\ S_{i+1,2j+1}\left(-D\frac{\partial P_{i+1,2j+1}(0,t)}{\partial x} + u_{i+1,2j+1}(t)P_{i+1,2j+1}(0,t)\right) \end{aligned} \tag{6}$$

where $S_{i,j} = \pi r_{i,j}^2$ is the cross section surface area of the branch j of generation i.

Furthermore, the air volumetric flow rate $q_{i,j} = u_{i,j}S_{i,j}$ in the airway (i,j) is also conserved through the bifurcation:

$$q_{i,j} = q_{i+1,2j} + q_{i+1,2j+1}.$$

Thanks to this equation and the continuity of the partial pressure P_i of the gas from one generation to the next, the gas mass conservation in the bifurcation is:

$$\begin{aligned} S_{i,j}\frac{\partial P_{i,j}(l_{i,j},t)}{\partial x} =& S_{i+1,2j}\frac{\partial P_{i+1,2j}(0,t)}{\partial x} \\ &+ S_{i+1,2j+1}\frac{\partial P_{i+1,2j+1}(0,t)}{\partial x}. \end{aligned} \tag{7}$$

Flow of gas exchanged with blood. Finally, the gas flow exchanged with blood is computed with

$$f_{\mathrm{O_2}} = \sum_{i=G}^{N}\frac{1}{T}\int_{t_C}^{t_C+T}\sum_{k=1}^{2^i}\int_0^{l_i}\gamma_{i,k}\times(P_{i,k}-P_{\mathrm{blood}})\,\mathrm{d}x\,\mathrm{d}t \tag{8}$$

where t_C is a time at which the system has reached a periodic regime and $\gamma_{i,k} = 2\pi r_{i,k}\alpha_i\rho_s$ with $r_{i,k}$ is the radius of the airway number k of the generation i. The quantity α_i is the permeability of the alveolar membrane, see equation (5) and ρ_s the amount of exchange surface area per unit of respiratory airway wall surface area.

Inflammation of the bronchi

The surface barriers are the first defenses of the innate immune system. In the lung, they consist in the mucus and in the ciliated cells [47]. We focus in this paper on the second defense of the innate immune system that responds once a pathogen has breached the surface barriers. This second defense is composed of chemicals and white blood cells, which are also called leucocytes [15].

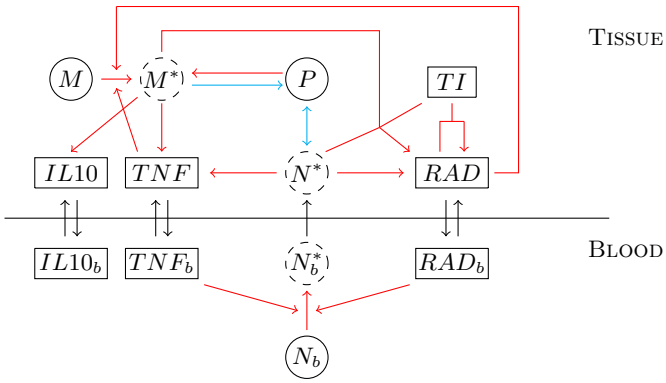

FIG. 3. Interactions of the immune system with the pathogens. Diffusion is represented by black arrows, up-regulation of immune interactions by red arrows and down-regulation of immune interactions by blue arrows. Reproduced from [28].

When the body detects pathogens in a tissue (P) or in blood (P_b), the first reaction of the immune system is to bring white blood cells (here macrophages and neutrophils) to the site of infection. When resting macrophages (M), already present in the tissue, come in contact with some pathogens, they become activated (M^*). Then, they can eliminate the pathogens and produce pro-inflammatory (TNF) and anti-inflammatory ($IL10$) cytokines. Pro-inflammatory cytokines migrate into blood (TNF_b) and send a signal to resting neutrophils (N_b) already present in blood. Once the signal is received by neutrophils, they become activated (N_b^*). These activated neutrophils have the ability to go into the tissue (N^*) and to fight the pathogens. Furthermore, during this infection, the tissue becomes inflamed (Z) and the presence of radicals (RAD and RAD_b), produced by activated macrophages and neutrophils, can damage the tissue that becomes less functional (TI). We choose to represent these interactions by using an existing model representing the response of the immune system in a human organ and its interplay with blood [28]. It describes the evolution of several variables that represent the response of the immune system in tissue and blood thanks to ordinary differential equations, as shown in Figure 3. We do not describe the whole infection model in this paper and we refer the reader to the work of A.M. Reynolds [28] for a detailed description. In this study, we use the same parameters values for the infection model as in [28].

In this paper, we focus on one particular variable of this infection model, the inflammation of the tissue Z. Its values range between 0 (no inflammation) and 1 (maximal inflammation). We assume that this amount of inflammation can be linked to the evolution of the bronchial volume (V_{br}) during an infection through the following function [20],

$$V_{\mathrm{br}}(Z) = \frac{V_{\mathrm{br,\ he}}}{1 + m_{vta} Z}, \tag{9}$$

where $V_{\mathrm{br,\ he}}$ is the volume of the healthy tissue and m_{vta} is a reduction parameter chosen equals to 1 as in [20]. By assuming that the bronchi are cylindrical, we can link this change of volume to the radius of the bronchus. Indeed, we know that the volume of a bronchus V_i of generation i can be computed as follow,

$$V_i = \pi r_i^2 l_i, \tag{10}$$

with r_i and l_i being respectively the radius and the length of the idealized cylindrical bronchus. Furthermore, since the length of the bronchus is not modified during an inflammation, we can replace this last expression in the equation (9). It leads to,

$$r_i(Z) = \frac{r_{i,\mathrm{he}}}{\sqrt{1 + m_{vta} Z}}, \tag{11}$$

where r_i is the inflamed radius and $r_{i,\mathrm{he}}$ is the healthy radius of the idealized bronchus of generation i.

Propagation of an infection

The dynamics of the spread of an infection throughout the bronchial tree can be very complex, with different propagation mechanisms: local growth of the infection, airborne propagation within the respiratory tract, propagation through the blood network or the epithelium, etc. The propagation mechanisms are specific to each infection and patient and depends on the pathogen characteristics, the geometry of the airways, the ventilation rate, etc. The mechanisms add together to create a complex dynamics. Here, we consider a pathogen that can develop locally in an airway and that can reach other airways by airborne propagation, a typical behavior of biofilms, viruses, etc. [48]. The probability of airborne propagation to other airways increases with the population of the pathogen inside the initial airway. We consider that the probability of infection of an airway depends on the probability of contact between a pathogen and the airway walls. At first approximation, we can consider that this probability is proportional to the number of airborne pathogens in the airway divided

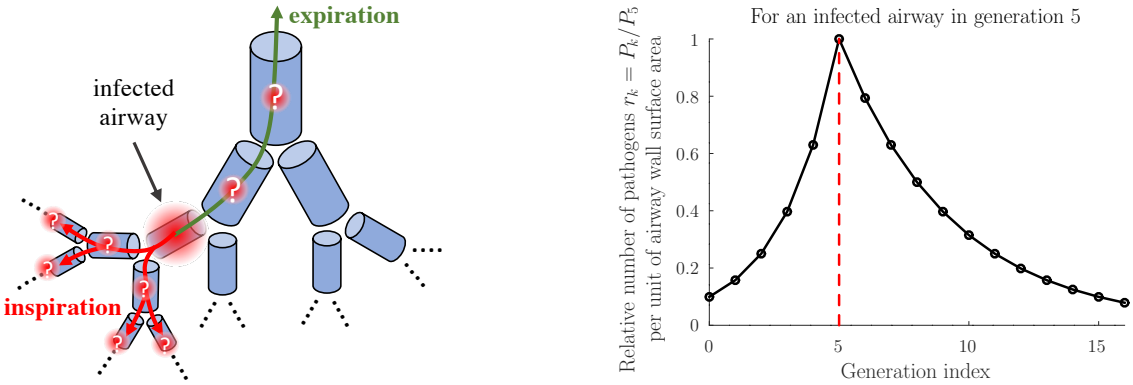

FIG. 4. **Left:** The airways with the red circles and the question mark are those visited by airborne pathogens originating from an infected airway during inspiration (red) and expiration (green). These airways are ought to become infected, but the pathogens dilute into larger volumes when going away from the infected airway. Consequently, the probability for an airway on the path of the pathogens to become infected decreases exponentially with the distance to the infected airway, as shown on the picture on the right. The other airways are not in direct contact with the pathogens as expiration expels all the airborne pathogens at each ventilatory cycle. **Right:** Example of the propagation of an airborne pathogen infecting an airway in the fifth generation. We assume that the probability of infection of an other airway is proportional to the number of pathogens in the airway per unit of airway wall surface area. During inspiration, the pathogens propagate in all the airways downstream the infected airway and the pathogens dilute into the volume of the numerous downstream airways. During expiration, the pathogens propagate in the airways on the path between the infected airway and the root of the tree (trachea), hence diluting itself into the volume of larger airways. Both situations lead to a number of pathogens per unit of airway wall surface decreasing exponentially with the distance to the infected airway. Hence, we assume in this work that the propagation is more likely to occur in a neighboring airway of the infected airway.

by the surface of the airway walls.

Propagation of the infection to other airways in a tree with symmetric bifurcations. Let us consider an airway in the generation i, which is infected with a pathogen and that the pathogen concentration in air is C_i. During expiration, the pathogens propagate to the upper airways on the path to the trachea. On that path, in the airway of the generation $i-n$, the concentration of the pathogens is given by mass conservation of the pathogens number: $C_i v_i S_i = C_{i-n} v_{i-n} S_{i-n} = 2^n C_{i-n} v_i S_i$. Finally,

$$C_{i-n} = C_i/2^n$$

If we denote $q_i = C_i(\pi r_i^2 l_i)/(2\pi r_i l_i) = C_i r_i/2$ the number of pathogens per unit of wall surface area in the infected airway of generation i, then

$$q_{i-n} = C_{i-n}\frac{\pi r_{i-n}^2 l_{i-n}}{2\pi r_{i-n} l_{i-n}} = C_{i-n}\frac{r_{i-n}}{2} = C_i\frac{r_i}{2(2h)^n} = \frac{1}{(2h)^n} q_i$$

Since $2h \simeq 1.6$, the number of pathogens per surface of airway walls decrease exponentially on the path to the trachea during expiration.

During inspiration, the pathogens propagate to all the airways below the infected airway. Mass conservation of the pathogens writes $C_i v_i S_i = 2^n C_{i+n} v_{i+n} S_{i+n} = C_{i+n} v_i S_i$. Finally,

$$C_{i+n} = C_i$$

Hence, the number of pathogens per unit of wall surface area is

$$q_{i+n} = C_{i+n}\frac{\pi r_{i+n}^2 l_{i+n}}{2\pi r_{i+n} l_{i+n}} = C_{i+n}\frac{r_{i+n}}{2} = C_i\frac{r_i h^n}{2} = h^n q_i$$

Since $h \simeq 0.8$, the number of pathogens per surface of airway walls decrease exponentially along the generations below the infected airway.

The time of residence t_k of the pathogens inside an airway does not depend on the generation index k as $t_k = l_k/v_k = (2h^3)^k l_0/v_0 = l_0/v_0 \simeq 0.06$ s. Hence, the pathogens in the airways spend the same time in contact with the airway wall whatever the generation.

Finally, the airborne pathogens from generation i are all expelled from the lung. Indeed, at rest, the time $t_{i\to 0}$ for air to get out of the airway tree from the generation i is about 1 s while the expiratory time T_e is of about 2–3 s at rest:

$$t_{i\to 0} = \sum_{k=0}^{i} t_k = (i+1)\frac{l_0}{v_0}$$
$$\simeq (i+1) \times 0.06 \text{ s } < 17 \times 0.06 \simeq 1 \text{ s } < T_e \simeq 2\text{–}3 \text{ s}$$

Hence, the previous analysis shows that due to mass conservation and to geometrical constraints of

the airway tree, the probability of infection actually decreases exponentially with the distance to the infected airway. Indeed, the airborne pathogens in the infected airways are transported to larger volumes, either up the tree where the airways are larger during expiration, or down the tree where the airborne pathogens dilute into a large number of airways during inspiration. Moreover, at each expiration and even at rest, the velocities of the air should drive most the pathogens out of the bronchial tree, to the ambient air.

Probability of infection of the neighboring airways of an infected airway. To mimic the propagation in a simple framework, we suppose that the infection has a probability to spread to its neighbor airway only (its mother airway and its two daughter airway), which are the more likely to become infected as explained above and in Figure 4. This probability depends on the amount of pathogens present in the airway. For simplicity, in a first approach, we assume that the newly infected airway will suffer from an infection that has the same initial and dynamical properties than the source infection.

We choose a probability function f_p with the following form,

$$f_p(P, P_s) = \begin{cases} \frac{1}{2}\left(\frac{2P}{P_s}\right)^2, & \text{for } P < \frac{P_s}{2}, \\ 1 - \frac{1}{2}\left(\frac{2(P_s - P)}{P_s}\right)^2, & \text{for } \frac{P_s}{2} \leqslant P < P_s, \\ 1, & \text{for } P > P_s. \end{cases} \tag{12}$$

P is the number of pathogen present in the bronchus and P_s is a parameter that represents the speed of the propagation. Actually, the lower this variable is, the faster the propagation. In our simulations, we use different P_s to model different speeds of infection proliferation, as shown in Figure 5. The shape of the functions of propagation has been chosen as a sigmoid. Such a shape assumes the necessity of a minimal threshold of pathogens for the infection to propagate to a new airway and a saturation effect with a probability of propagation close to 1 when the number of pathogens overcomes is large enough. This choice is based on the observed shape of the function of propagation between individuals versus viral charge for Covid19 [49].

NUMERICAL SIMULATIONS

A detailed description of the simulations and of the values of the parameters are available in Appendix C. The model equations are solved using the software Julia [50]. The algorithm is decomposed into two steps.

The first step aims at solving the infection equations independently of the airways. The infection dynamics is assumed to be the same in all the infected airways, but with shifted starting time. Actually, the starting time of the infection depends on when the airway is infected by its neighbours. Next, we compute the propagation of the infection in the airway tree. The output of the first step is the list of the infected airways with their inflammation degree Z for each time step.

The second step computes the oxygen transport in the infected airway tree. From the inflammation degree Z, the radii, hydrodynamic resistance of the airways and airflows in the airways are computed. Then, the path types are computed, and the oxygen transport equations are normalized and solved in each path type using finite differences. Then the oxygen partial pressure in the whole tree is reconstructed from the results obtained from each path types and the oxygen flow to blood is computed.

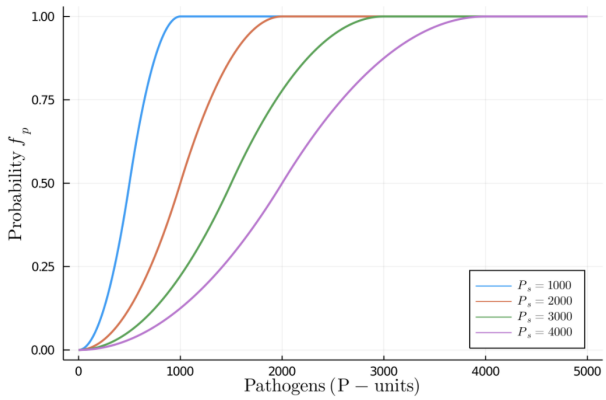

FIG. 5. Probability functions for the propagation of infections to a neighbor of an infected airway. Each curve corresponds to a different value of the parameter P_s, see equation (12). The lower is the value of P_s, the higher is the infection rate.

RESULTS

Pulmonary infections can be limited to certain parts of the lung. For example, pneumonia affects mainly the alveoli and bronchitis affects mainly the first generations of the bronchial tree [3]. In this work, we focus on infections affecting the proximal airways only. More precisely, we assume that the infection is limited to the nine first generations of the lung. Limiting the number of potentially infected airways allows our numerical simulations to be performed with a reasonable computation time.

In the following, we assume that the infection starts in an airway of the fourth generation. Since the propagation of the infection is driven by the probability function f_p, see equation (12), the model is stochastic and the results of the simulations vary, even for the same set of parameters. Nevertheless, a large set of simulations allow to extract several characteristical behaviors of the

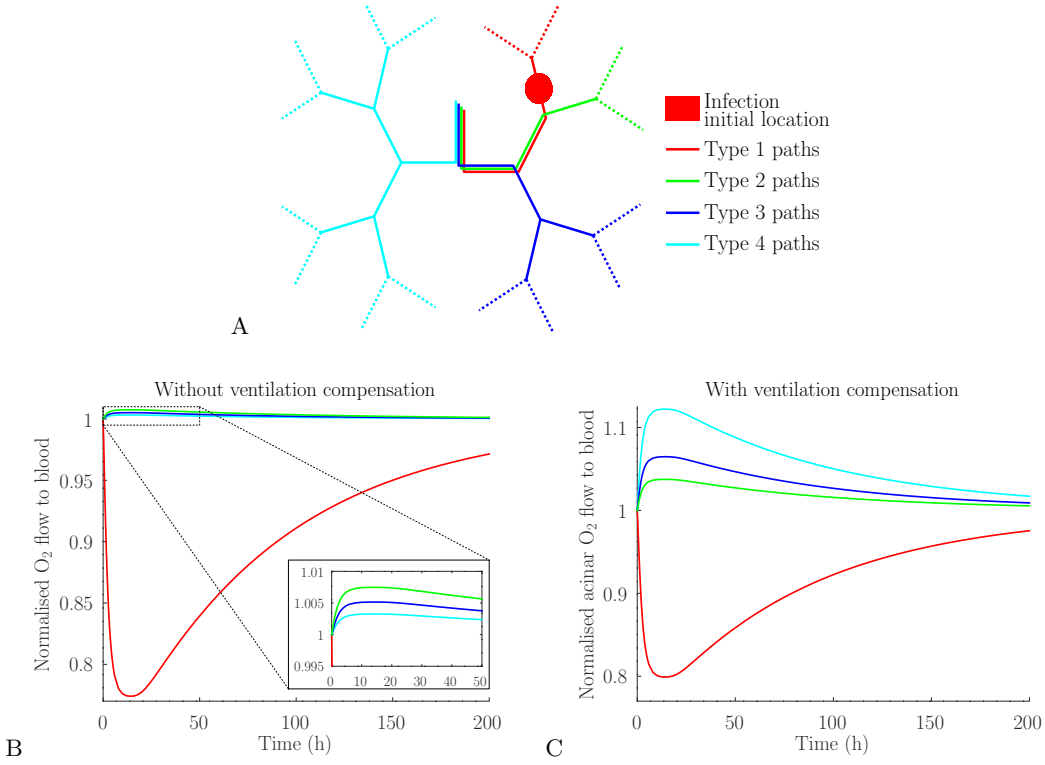

FIG. 6. Simulation of an infection limited to a single airway in the fourth generation. **A:** The tree is decomposed into four path types between the root of the tree and the terminal airways of the tree. The red circle corresponds to the infected airway. Paths of the same type have the same physical and geometrical properties and brings the same amount of oxygen to the blood. In this specific case, four types of paths exist, each of them is represented with a single color (red, green, clear and dark blue). **B:** Amounts of oxygen transferred to blood for each path type in the case where the energy spent for ventilation remains the same as the healthy state (no compensation by the ventilation). **C:** Amounts of oxygen transferred to blood for each path type in the case where ventilation is modified to keep the amount of oxygen to blood equal to that of the healthy state.

system. We analyse most particularly the effect of the airways inflammation on the oxygen flow to blood. In order to be able to compare the effect of the infection with the healthy state, we assume in general that the energy spent by the respiratory muscles is not modified by the infection. This condition is mimicked by applying the same pressure in the terminal airways.

Three different outcomes for the infection were simulated. The first one is a cured outcome, where the pathogens are quickly eliminated by the immune system. The tissue recovers after the inflammation and goes back to a healthy state. This outcome corresponds to an initial number of pathogens ranging between 0 and 840 P-units. In our case, we choose an initial number of 500 P-units, as suggested in [28]. The second outcome simulated is an aseptic death. In this case, the immune system succeeds to remove all the pathogens. However, the immune response is so intense that the tissue does not recover and stays inflamed. This outcome results from an initial number of pathogens ranging between 840 and 1060 P-units. In our case, we choose an initial number of 850 P-units, as suggested in [28]. Finally, the last outcome is a septic death, where there are too many pathogens for the immune system, which fails to cure the infection. This outcome results from an initial number of pathogens superior to 1060 P-units. In our case, we choose an initial number of 1200 P-units, as suggested in [28].

Single branch infection

We start with the case of a single infected airway in the fourth generation and we assume that the infection does not spread to the other airways. Furthermore, we suppose that the infected airway is in a configuration of a cured outcome, i.e. P is initialized to 500 P-units.

Our model predicts that the development of the inflammation during the first hours of the infection reduces the oxygen flow to blood if there is no compensation by the ventilation, see Figure 6B. The lumen surface area of the inflamed airway decreases, which induces the increase of the hydrodynamic resistance of the airway tree. The air flow in the inflamed region and in the whole tree is decreased, as predicted by the equation (2).

Moreover, the distribution of the airflows in the airways is modified, see Figure 6B,C. The type 1 paths in-

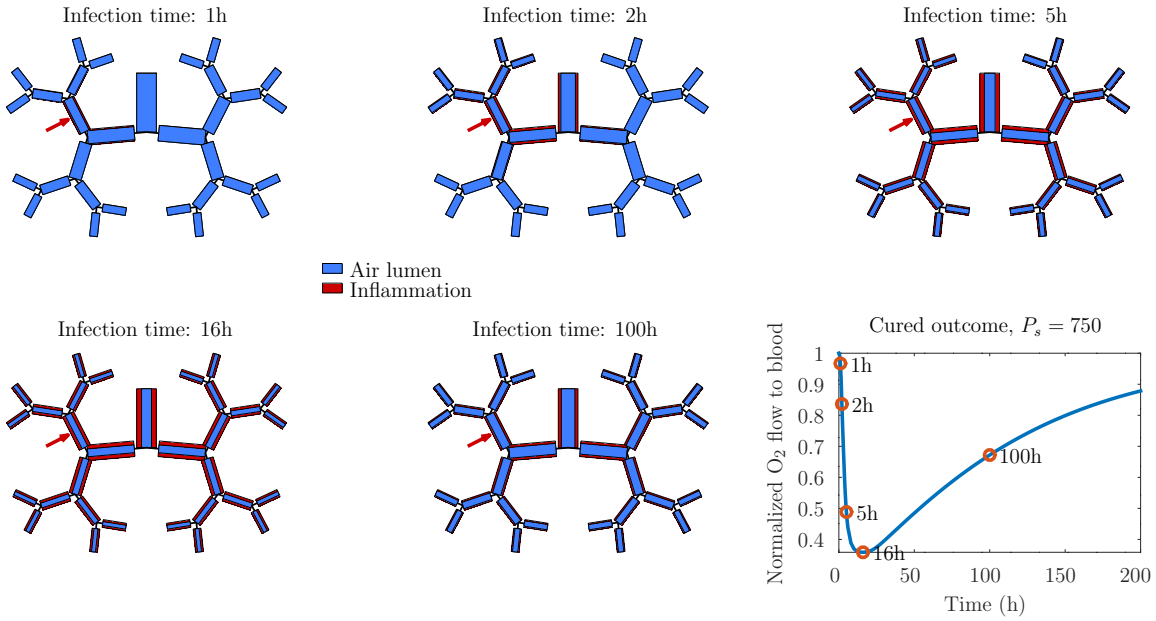

FIG. 7. Exemple of the propagation of an infection with a cured outcome and $P_s = 750$ (replicate number 12). The red arrow indicate the airway of generation three from which the infection originates. In this simulation, the infection is limited to the five first generations. The rectangles represent the airways, with respected proportions between lengths and widths and between the different airways. The surface area ratio of red over blue represents the proportion of the airways section surface area that is obstructed by the inflammation. The infection propagates and develops into the airways progressively and start recessing from hour 16. At hour 16 the tree reaches its largest obstruction and the oxygen flow to blood is decreased by more than 60%.

clude the inflamed airway and their inner airflows decrease. The convection–diffusion transition on these paths recesses and the ventilation of the downwards acini is decreased. The transition between an oxygen transport by convection and a transport by diffusion is localized near the entry of the acini for humans at rest, in the healthy case [29, 30]. The action length of diffusion in a tree structure is limited [51] and the localization of the transition has to be close enough to the entry of the acini for oxygen to access properly the exchange surface. The decrease of the airflow moves this transition to the conductive part of the tree and the exchange surface becomes far less accessible for oxygen. Hence, the transfer of oxygen to blood is drastically reduced on these paths.

The types 2, 3 and 4 paths do not include the inflamed airway. The case without a compensation of the oxygen loss by a change in the ventilation is plotted in Figure 6B. In the types 2, 3 and 4 paths, the airflow increases slightly in comparison with the healthy case, all the more in the paths that are closer to the inflamed airway. For these path types, the convection–diffusion transition progresses slightly deeper in the tree and the ventilation of the downwards acini is slightly increased. The total airflow is however reduced and the recess of the convection–diffusion transition in the obstructed pathways is much larger than the progression of the transition in the non obstructed pathways. Hence, the global oxygen flow to blood is decreased.

This behavior can be described mathematically by representing the tree with the resistance of the first generation $R_{0,0}$ and the resistance R_1 and R_2 of the two subtrees stemming from the first generation. When the tree is not inflamed, we assume $R_2 = R_1$ and during inflammation, the subtree corresponding to R_2 is obstructed and $R_2 > R_1$. The equivalent resistance of the non inflamed tree is $R_{\mathrm{He}} = R_0 + R_1/2$, its global air flow is $Q_{\mathrm{He}} = \Delta p/R_{\mathrm{He}}$. The resistance of the inflamed tree is $R = R_0 + R_1R_2/(R_1 + R_2)$ and its global air flow is $Q = \Delta p/R < Q_{\mathrm{He}}$. With the inflamed airway, the convection–diffusion transition shifts from generations $k_{1,\mathrm{He}}$ and $k_{2,\mathrm{He}}$ to generations k_1 and k_2. For human at rest, $k_{1,\mathrm{He}} = k_{2,\mathrm{He}} \simeq 16$. Hence, the transition shifts deeper in the acini in the subtree with resistance R_1 and upper in the conductive tree for the subtree with resistance R_2. We can compute the shifts in generations of the transition,

$$\begin{aligned} k_1 &= 16 + \delta_1 \text{ with } \delta_1 = \frac{\log\left(\frac{2R_2}{R_1+R_2}\frac{R_{\mathrm{He}}}{R}\right)}{\log(2h)} > 0 \\ k_2 &= 16 - \delta_2 \text{ with } \delta_2 = -\frac{\log\left(\frac{2R_1}{R_1+R_2}\frac{R_{\mathrm{He}}}{R}\right)}{\log(2\times 1)} > 0 \end{aligned} \tag{13}$$

A simple analysis shows that $\delta_1 > 0$ and $\delta_2 > 0$, and also that $\delta_1 < \delta_2$. Moreover, $\delta_1 \overset{R_2 \to +\infty}{\longrightarrow} \frac{\log(R_{\mathrm{He}}/R)}{\log(2h)}$ and $\delta_2 \overset{R_2 \to +\infty}{\longrightarrow} +\infty$. Hence, the exchange surface gained in the subtree 1 is not able to compensate the exchange surface lost in the subtree 2. The lack of compensation increases when R_2 increases. This analysis can be easily extended to any bifurcation of the airway tree and explains why the oxygen flow to blood decreases when R_2 increases.

Figure 6C shows the case of a ventilation that is adjusted to keep the amount of oxygen flow to blood at the healthy state level. The smaller is the hydrodynamic resistance of a path, the larger the airflow. The oxygen flow lost in the type 1 paths, which include the inflamed airway, is compensated by shifting the location of the convection–diffusion transition deeper in the other path types, hence recruiting in these regions a larger exchange surface. Nevertheless, as the global hydrodynamic resistance of the tree is increased, the compensation by ventilation goes with a larger energy cost of ventilation, which might strained the patient out.

When the inflammation starts to decline, the airway lumens reopen and the oxygen flow starts to increase back toward its healthy value.

Computations with carbon dioxide showed that the evolutions of the flow of carbon dioxide from blood are very similar to those of oxygen. Hence, we focus only on the oxygen flow in this paper.

Whole tree infection

Figure 7 shows an example of the inflammation during an infection starting from an airway of the third generation and limited to the five first generations, for visualization purpose. The infection represented on that figure corresponds to a cured outcome with $P_s = 750$. As P_s is small the infection propagates quickly and reaches all the airways susceptible to the infection. The inflammation obstructs the airways and induces a drop in the air flow entering the tree, which in turn induces a drop in the transfer of oxygen to blood. The inflammation is represented for different times, which correspond to different decrease of the oxygen flow, as indicated in the bottom right plot of Figure 7. In this example, at the maximal infection intensity, the oxygen flow to blood is reduced by more than 60%. Hence, hypoxia – a lack of oxygen in blood – is most probably induced. In these simulations, the pressure drop through the airway tree is still assumed constant, to allow easier comparisons between the different cases. This hypothesis corresponds to respiratory muscles applying the same force to the lung whatever the degree of infection. However, the response

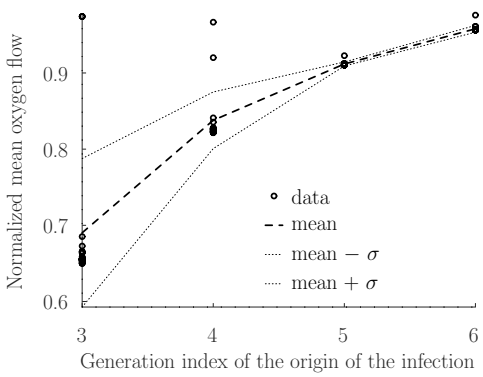

FIG. 8. Mean oxygen flow to blood during an infection as a function of the generation index of the first infected airway. The infection is limited to a range of five generations centered on the generation of the first infected airway. The deeper the infection, the larger is the reserve of exchange surface in the acini connected to the non infected airways. Hence, with our model hypotheses, the deeper the infection, the less the oxygen flow to blood is affected by the airway inflammation.

of the respiratory system to hypoxia is to increase the ventilation rate and amplitude in order to compensate the loss of oxygen [29, 52]. The physiological response increases the energetic cost of ventilation. Even in the case where it is able to compensate the loss of oxygen, it is a source of fatigue for the organism, which adds to the fatigue due to the immune response to the infection.

The depth of the inflamed generations plays an important role. We studied infections limited to a range of five generations around the one of the first infected airway. We plotted in Figure 8 the mean oxygen flow to blood during the infections as a function of the generation of first infected airway. The oxygen flow to blood is far more affected for infections that originate from the upper generations (small generation index) than from the deep generations (large generation index). Actually, the upper is the inflammation, the larger the number of paths and acini affected by the obstruction.

To get more general insights on the inflammation process, we simulated a set of infections that can propagate to the first 9 generations of the airway tree. The three outcomes (cured, septic and aseptic death) were simulated with values of P_s ranging from 750 to 4000 with steps of 250. As the dynamics of propagation is stochastic, we simulated 20 replicates (individuals) of each couple of parameters configurations. Our results show that most of the infections either are limited to a small number of airways, or, on the contrary, propagate to all the 511 airways, which are susceptible to the infection, as shown in Figure 9A. Indeed, each newly infected airway becomes a new possible source of infection for its neighboring uninfected airways. Hence, the more the infection propagates throughout the airway tree, the larger is the

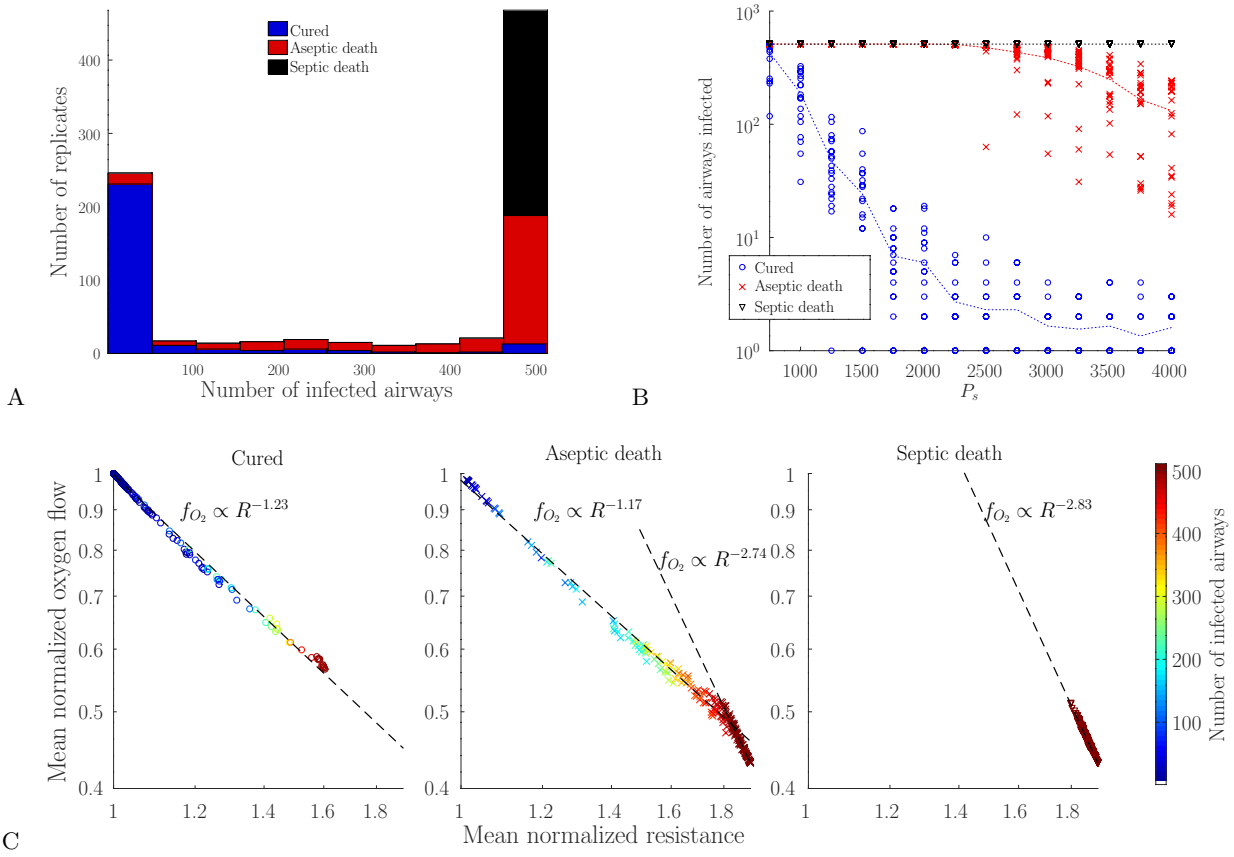

FIG. 9. **A:** Number of airways infected for all the possible outcomes for infections limited to the 9 first generations, i.e. the maximal number of infected airways is 511. Most of the infections are either limited to a few airways or propagate to the all the airways that are susceptible to the infection. **B:** Number of airways infected as a function of the value of P_s and of the outcome for infections limited to the 9 first generations. The propagation in the airway tree is reflected by the number of infected airways. The capacity of the infection to propagate is directly dependent on the number of pathogens infecting the airways. The cured outcome has less pathogens than the aseptic death outcome, which has less pathogens than the septic death outcome. **C:** Dependence of the time-averaged oxygen flow to blood f_{O_2} to the time-averaged equivalent hydrodynamic resistance of the airway tree. Both quantities are averaged over the duration of the infection. Each circle represents a replicate and the circle color represents the corresponding value of P_s. The averaged oxygen flow to blood follows a power law in the averaged hydrodynamic resistance. There are two regimes: a regime at low and medium hydrodynamic resistance and a regime at high hydrodynamic resistance.

pool of uninfected airways reachable by the infection and the propagation dynamics amplifies.

Higher P_s values corresponds to infections that are less prone to propagate between the airways. Accordingly, the number of infected airways is lower than for high values of P_s than for small ones, as shown in Figure 9B. Moreover, if the immune system is able to reduce effectively and quickly enough the number of pathogens in the airways, as in the cured outcome, then the infection is less prone to propagate in the airway tree. Hence, in the case of the cured outcome, only highly contagious infections (low values of P_s) are able to infect the whole tree. On the contrary, for the septic death outcome, the immune system is not able to eliminate the pathogens and the whole tree is always infected, even for high values of P_s. The aseptic death outcome stands in between the cured and septic death outcomes and its behavior is more dependent on the value of P_s.

Actually, with our model hypotheses, the degree of inflammation of the airways and its influence on the airflow and, consequently, on the oxygen flow to blood can be represented by the equivalent hydrodynamic resistance of the whole tree. Typically, a high hydrodynamic resistance will be correlated to a lower air flow and to a larger drop in the oxygen flow to blood. We analyse the effect of the tree obstruction, i.e. the tree resistance R, on the oxygen flood to blood f_{O_2} in Figure 9C. We observed a power law linking f_{O_2} to R, of the type $f_{O_2} \propto R^{-a}$ with $a > 0$. The value of a is about $1.24 - 1.29$ for light and medium increase of the tree resistance and is

about $2.63 - 2.76$ for large increase of resistance, mainly the cases where the infection is able to propagate in the whole tree. These exponents are related to the efficiency of the capture of oxygen from the air flow inhaled and to the inhomogeneity of the ventilation of the acini. Actually, the resistance is more strongly affected by the obstruction of upper airways than deeper airways. Indeed, less pathways to the exchange surface are affected by the obstruction of deeper airways than by the obstruction of upper airways, as shown in Figure 8. Hence, the exponents are related to the obstruction level of the airway tree. The shift from $1.24 - 1.29$ to $2.63 - 2.76$ is occurring at large resistance increase, of about a factor 1.8. Such an increase corresponds to infections that reach the trachea, and consequently affects all the pathways to the exchange surface. As a consequence, the oxygen flow to blood is drastically reduced.

DISCUSSION

In this work, we model a generic infection of the bronchial tree that originates from a single airway and that propagates from one airway to its neighbors. In order to understand the effect of the inflammation on the oxygen transfer to blood, we study the links between the propagation of the infection throughout the lung and the redistribution of the air flows between the airways. To be able to compare the different steps of the infection, we assume in most of our simulations that the lung is ventilated with the same work at any time during the infection.

Our model is based on several simplification hypotheses that need to be accounted for in any interpretations of the model. In this work, the infection is assumed to originate from a single airway and its propagation is done step-by-step and limited at each step to the neighboring airways of the infected airways. Moreover, the dynamics of the infection is assumed similar in all the airways, with the same initial number of pathogens at the beginning of the infection of an airway. Actually, the dynamics of an infection depends on the type of infection and is far more complex as it involves many other mechanisms, which are not accounted for in this work. Nevertheless, our study should be considered as a first step towards the understanding of the propagation dynamics of an infection in the lung.

In our knowledge, no data about the infection dynamics within the lung is available in the literature. However, global predictions of our model can be compared with typical symptoms of frequent respiratory diseases. For example, our results compare qualitatively well with the pathophysiology of influenza [53]. Influenza has a severity that can range from benign to critical and that is linked, at least partially, to the degree of inflammation. The more acute infection leads to hypoxia – low oxygenated blood. In this case, the response of the control of ventilation is to increase the ventilation rate and tidal volume, eventually adding to the fatigue due to hypoxia. These symptoms and how increased ventilation improves the oxygenation are predicted by our model and form typical criteria for influenza patients triage in emergency service [53]. To avoid exhaustion and/or respiratory failure, compensating strategies could be implemented, such as intubation and mechanical ventilation [53, 54].

Our model allows to get detailed insights on the dynamics of an inflammation on the oxygen exchanges with the blood. The obstruction of certain pathways that connect the exchange surface with blood to the ambiant air reduces the total air flow in the tree, but increases the air flows in the non obstructed pathways. This phenomenon allows to compensate the oxygen loss when the ventilation is adjusted to keep the oxygen flow at healthy rate. When the ventilation is not adjusted, this phenomenon still exists, but remains marginal. This compensation effect is affected by the generation index of the inflamed airways. The exchange surface affected by the obstruction of the airways is larger when the generations indexes of the inflamed airways are smaller. This dynamics suggests that the oxygen flow exchanged with blood is not only related to the number of airways infected, but also to the depth of the infection in the tree. Hence, in the frame of our model hypotheses, preventing the infection to reach the large airways is a way to limit the drop of the oxygen flow to blood during the infection.

CONCLUSION

We develop a first approximation model a generic infection of the bronchial tree that propagates from one airway to its neighbors. Our results suggest that the resulting inflammation of the airways could drastically affect the oxygen flow to blood. Moreover, our study allows to relate the distribution of the obstructions with the reorganization of the air flows in the airway tree and with the oxygen flow to blood. We highlight the condition for the existence of a compensation mechanism induced by the air fluid mechanics in the airway tree. This work represents a first step towards the understanding of the behaviors of the oxygen exchange with blood during a bronchial infection. Future works should focus on improving the model of propagation of the infection between the airways and on considering different infection dynamics for each airway. Moreover, our model could form the basis of models dedicated to the study of the propagation of specific infections in the lung, such as pneumonia or COVID19.

ACKNOWLEDGEMENT

This research has been supported by the Agence Nationale de la Recherche (VirtualChest project, ANR-16-CE19-0014; IDEX UCA JEDI, ANR-15-IDEX-01).

[1] E. R. Weibel, *The Pathway for Oxygen: Structure and Function in the Mammalian Respiratory System*. Harvard University Press, 1984.

[2] J. P. Mizgerd, "Lung Infection—A Public Health Priority," *PLoS Med*, vol. 3, p. e76, Jan. 2006.

[3] J. F. Murray and J. A. Nadel, *Textbook of respiratory medecine*. Elsevier, 6 ed., 2016.

[4] M. Malouf and A. Glanville, "The Spectrum of Mycobacterial Infection after Lung Transplantation," *Am J Respir Crit Care Med*, vol. 160, pp. 1611–1616, Nov. 1999.

[5] J. R. W. Govan and J. W. Nelson, "Microbiology of lung infection in cystic fibrosis," *British Medical Bulletin*, vol. 48, no. 4, pp. 912–930, 1992.

[6] D. Dreyfuss and J.-D. Ricard, "Acute Lung Injury and Bacterial Infection," *Clinics in Chest Medicine*, vol. 26, pp. 105–112, Mar. 2005.

[7] M. R. Stämpfli and G. P. Anderson, "How cigarette smoke skews immune responses to promote infection, lung disease and cancer," *Nat Rev Immunol*, vol. 9, pp. 377–384, May 2009. Bandiera_abtest: a Cg_type: Nature Research Journals Number: 5 Primary_atype: Comments & Opinion Publisher: Nature Publishing Group.

[8] T. P. Velavan and C. G. Meyer, "The COVID-19 epidemic," *Tropical Medicine & International Health*, vol. 25, pp. 278–280, Mar. 2020.

[9] L. Li, Q. Huang, D. C. Wang, D. H. Ingbar, and X. Wang, "Acute lung injury in patients with COVID-19 infection," *Clinical and Translational Medicine*, vol. 10, pp. 20–27, Jan. 2020.

[10] H. Ritchie, E. Ortiz-Ospina, D. Beltekian, E. Mathieu, J. Hasell, B. Macdonald, C. Giattino, and M. Roser, "Coronavirus (COVID-19) cases." `https://ourworldindata.org/covid-cases`, 2020.

[11] M. King, "Physiology of mucus clearance," *Paediatric Respiratory Reviews*, vol. 7, pp. S212–S214, Jan. 2006.

[12] P. J. Basser, T. A. McMahon, and P. Griffith, "The mechanism of mucus clearance in cough," *Journal of biomechanical engineering*, vol. 111, no. 4, pp. 288–297, 1989.

[13] M. R. Knowles and R. C. Boucher, "Mucus clearance as a primary innate defense mechanism for mammalian airways," *Journal of Clinical Investigation*, vol. 109, pp. 571–577, Mar. 2002.

[14] M. Munkholm and J. Mortensen, "Mucociliary clearance: pathophysiological aspects," *Clin Physiol Funct Imaging*, vol. 34, pp. 171–177, May 2014.

[15] E. N. Marieb and K. N. Hoehn, *Human anatomy and physiology*. Pearson, 11 ed., 2018.

[16] J. Day, A. Friedman, and L. S. Schlesinger, "Modeling the immune rheostat of macrophages in the lung in response to infection," *Proceedings of the National Academy of Sciences*, vol. 106, pp. 11246–11251, July 2009. Publisher: National Academy of Sciences Section: Biological Sciences.

[17] W. Hao, E. D. Crouser, and A. Friedman, "Mathematical model of sarcoidosis," *Proceedings of the National Academy of Sciences of the United States of America*, vol. 111, pp. 16065–16070, Nov. 2014.

[18] D. Gammack, C. R. Doering, and D. E. Kirschner, "Macrophage response to Mycobacterium tuberculosis infection," *Journal of Mathematical Biology*, vol. 48, pp. 218–242, Feb. 2004.

[19] F. Clarelli and R. Natalini, "A pressure model of immune response to mycobacterium tuberculosis infection in several space dimensions," *Mathematical biosciences and engineering: MBE*, vol. 7, pp. 277–300, Apr. 2010.

[20] A. Reynolds, G. Bard Ermentrout, and G. Clermont, "A mathematical model of pulmonary gas exchange under inflammatory stress," *Journal of Theoretical Biology*, vol. 264, pp. 161–173, May 2010.

[21] H. Mayer, K. S. Zaenker, and U. An Der Heiden, "A basic mathematical model of the immune response," *Chaos (Woodbury, N.Y.)*, vol. 5, pp. 155–161, Mar. 1995.

[22] A. S. Perelson, "Modelling viral and immune system dynamics," *Nature Reviews. Immunology*, vol. 2, pp. 28–36, Jan. 2002.

[23] D. Wodarz, "Mathematical models of immune effector responses to viral infections: Virus control versus the development of pathology," *Journal of Computational and Applied Mathematics*, vol. 184, pp. 301–319, Dec. 2005.

[24] A. Reynolds, J. Rubin, G. Clermont, J. Day, Y. Vodovotz, and G. Bard Ermentrout, "A reduced mathematical model of the acute inflammatory response: I. Derivation of model and analysis of anti-inflammation," *Journal of Theoretical Biology*, vol. 242, pp. 220–236, Sept. 2006.

[25] L. Caudill and F. Lynch, "A Mathematical Model of the Inflammatory Response to Pathogen Challenge," *Bulletin of Mathematical Biology*, vol. 80, no. 8, pp. 2242–2271, 2018.

[26] A. Murase, T. Sasaki, and T. Kajiwara, "Stability analysis of pathogen-immune interaction dynamics," *Journal of Mathematical Biology*, vol. 51, pp. 247–267, Sept. 2005.

[27] A. M. Elaiw, A. Alhejelan, and M. A. Alghamdi, "Global Dynamics of Virus Infection Model with Antibody Immune Response and Distributed Delays," *Discrete Dynamics in Nature and Society*, vol. 2013, pp. 1–9, 2013. Publisher: Hindawi.

[28] A. M. Reynolds, *Mathematical Models of Acute Inflammation and a Full Lung Model of Gas Exchange Under Inflammatory Stress*. phdthesis, University of Pittsburg, 2008.

[29] F. Noël and B. Mauroy, "Interplay Between Optimal Ventilation and Gas Transport in a Model of the Human Lung," *Front. Physiol.*, vol. 10, 2019.

[30] F. Noël, C. Karamaoun, J. A. Dempsey, and B. Mauroy, "The origin of the allometric scaling of lung ventilation in mammals," *Peer Community Journal*, vol. 2, 2022.

[31] F. Noël, *Influence of the ventilation on the transport properties in the healthy and inflamed lung*. PhD thesis, Université Côte d'Azur, Nice, France, 2021.

[32] B. Mauroy, M. Filoche, E. R. Weibel, and B. Sapoval, "An optimal bronchial tree may be dangerous," *Nature*, vol. 427, pp. 633–636, Feb. 2004.

[33] B. Mauroy, C. Fausser, D. Pelca, J. Merckx, and P. Flaud, "Toward the modeling of mucus draining from the human lung: role of the geometry of the airway tree," *Physical Biology*, vol. 8, p. 056006, Oct. 2011.

[34] B. Mauroy, P. Flaud, D. Pelca, C. Fausser, J. Merckx, and B. R. Mitchell, "Toward the modeling of mucus draining from human lung: role of airways deformation on air-mucus interaction," *Front. Physiol.*, vol. 6, 2015.

[35] R. Eccles, "Understanding the symptoms of the common cold and influenza," *Lancet Infect Dis*, vol. 5, pp. 718–725, Nov. 2005.

[36] M. Thomas and P. A. Bomar, "Upper Respiratory Tract Infection," in *StatPearls*, Treasure Island (FL): StatPearls Publishing, 2022.

[37] E.-Y. Kang, "Large Airway Diseases," *Journal of Thoracic Imaging*, vol. 26, pp. 249–262, Nov. 2011.

[38] T. J. Pedley, R. C. Schroter, and M. F. Sudlow, "The prediction of pressure drop and variation of resistance within the human bronchial airways," *Respiration Physiology*, vol. 9, pp. 387–405, June 1970.

[39] M. Florens, B. Sapoval, and M. Filoche, "Optimal Branching Asymmetry of Hydrodynamic Pulsatile Trees," *Phys. Rev. Lett.*, vol. 106, p. 178104, Apr. 2011.

[40] J. Stéphano and B. Mauroy, "Wall shear stress distribution in a compliant airway tree," *Physics of Fluids*, vol. 33, p. 031907, Mar. 2021. Publisher: American Institute of Physics.

[41] B. Mauroy, M. Filoche, J. S. Andrade, and B. Sapoval, "Interplay between geometry and flow distribution in an airway tree," *Physical Review Letters*, vol. 90, p. 148101, Apr. 2003.

[42] B. Mauroy and N. Meunier, "Optimal Poiseuille flow in a finite elastic dyadic tree," *ESAIM: Mathematical Modelling and Numerical Analysis*, vol. 42, pp. 507–533, July 2008.

[43] B. Mauroy and P. Bokov, "The influence of variability on the optimal shape of an airway tree branching asymmetrically," *Phys Biol*, vol. 7, no. 1, p. 16007, 2010.

[44] X. Dubois de La Sablonière, B. Mauroy, and Y. Privat, "Shape minimization of the dissipated energy in dyadic trees," *Discrete and Continuous Dynamical Systems - Series B, American Institute of Mathematical Sciences*, 2011.

[45] A. J. Chorin and J. E. Marsden, *A mathematical introduction to fluid mechanics*. Texts in applied mathematics, New York: Springer-Verlag, 1990.

[46] M. Felici, *Physics of the oxygen diffusion in the human lung*. PhD thesis, Ecole Polytechnique X, June 2003.

[47] J. V. Fahy and B. F. Dickey, "Airway Mucus Function and Dysfunction," *The New England journal of medicine*, vol. 363, pp. 2233–2247, Dec. 2010.

[48] P. Chakraborty, S. Bajeli, D. Kaushal, B. D. Radotra, and A. Kumar, "Biofilm formation in the lung contributes to virulence and drug tolerance of Mycobacterium tuberculosis," *Nat Commun*, vol. 12, p. 1606, Mar. 2021. Bandiera_abtest: a Cc_license_type: cc_by Cg_type: Nature Research Journals Number: 1 Primary_atype: Research Publisher: Nature Publishing Group Subject_term: Bacterial pathogenesis;Biofilms;Clinical microbiology;Pathogens Subject_term_id: bacterial-pathogenesis;biofilms;clinical-microbiology;pathogens.

[49] A. Marc, M. Kerioui, F. Blanquart, J. Bertrand, O. Mitjà, M. Corbacho-Monné, M. Marks, and J. Guedj, "Quantifying the relationship between SARS-CoV-2 viral load and infectiousness," *eLife*, vol. 10, p. e69302, Sept. 2021. Publisher: eLife Sciences Publications, Ltd.

[50] J. Bezanson, A. Edelman, S. Karpinski, and V. B. Shah, "Julia: A fresh approach to numerical computing," *SIAM review*, vol. 59, no. 1, pp. 65–98, 2017. Publisher: SIAM.

[51] B. Sapoval, M. Filoche, and E. R. Weibel, "Smaller is better—but not too small: A physical scale for the design of the mammalian pulmonary acinus," *PNAS*, vol. 99, pp. 10411–10416, June 2002.

[52] L. J. Teppema and A. Dahan, "The Ventilatory Response to Hypoxia in Mammals: Mechanisms, Measurement, and Analysis," *Physiological Reviews*, vol. 90, pp. 675–754, Apr. 2010.

[53] J. Rello and A. Pop-Vicas, "Clinical review: Primary influenza viral pneumonia," *Crit Care*, vol. 13, p. 235, Dec. 2009.

[54] J. S. Whittle, I. Pavlov, A. D. Sacchetti, C. Atwood, and M. S. Rosenberg, "Respiratory support for adult patients with COVID-19," *Journal of the American College of Emergency Physicians Open*, vol. 1, no. 2, pp. 95–101, 2020. _eprint: https://onlinelibrary.wiley.com/doi/pdf/10.1002/emp2.12071.

[55] R. Hill, H. P. Wolvekamp, and F. G. Hopkins, "The oxygen dissociation curve of haemoglobin in dilute solution," *Proc. R. Soc. Lond. B*, vol. 120, no. 819, pp. 484–495, 1936.

Appendix

A- Parameters values

Quantity	Value	Notation	Reference
Lungs' geometrical data			
healthy trachea radius	0.01 m	$r_{0,\mathrm{He}}$	[1]
trachea length (reduced)	0.06 m	l_0	[1]
bronchial tree reduction factor	$(1/2)^{\frac{1}{3}} \sim 0.79$	h	[1, 32]
resp. airways radius	0.01 m	$r_{0,\mathrm{He}}$	[1]
number of generations of conductive airways	17	G	[1]
number of generations of resp. airways	6	H	[1]
total number of generations	23	$N = G + H$	[1]
air–blood membrane thickness in alveoli	10^{-6} m	τ	[1]
Oxygen transport properties			
oxygen diffusion coefficient in air	$0.2\,10^{-4}$ m^2.s^{-1}	D	[51]
oxygen diffusion coefficient in water	$3.3\,10^{-9}$ m^2.s^{-1}	$D_{\mathrm{O_2,H_2O}}$	–
ratio between partial pressure of O_2 to its concentration in water	19.34 mmHg.mol^{-1}.m^3	k	–
solubility coefficient of oxygen in water	$1.34\,10^{-3}$ mol.m^{-3}.mmHg^{-1}	$\sigma_{\mathrm{O_2,H_2O}}$	–
amount of exchange surface area per unit of resp. airway wall surface area	9.29	ρ_s	[30]
Ventilation properties			
ventilation period	5 s	T	[1]
healthy ventilation amplitude	1.2 m.s^{-1}	A_{He}	[1]
Numerical parameters			
spatial step normalized relatively to the airway length	0.03	dx	–
time step	0.025 s	dt	–

TABLE I. Model and numerical parameters.

B- Oxygen partial pressure in blood

To determine the value of the oxygen partiel pressure in blood as a function of the oxygen partial pressure in the alveoli, we use the same approach proposed in [46], see more detailed in our previous models in [29, 30] We assume that the oxygen flow going out of the alveoli is equal to the oxygen flow carried away by the blood. The blood oxygen is stored in haemoglobin and dissolved in plasma, it is carried away by the blood flow. Consequently, the flow balance is

$$\alpha\,(P_{i,j} - P_{\mathrm{blood}}) = 4Z_0(f(P_{\mathrm{blood}}) - f(\tilde{P}_{aO_2})) + \sigma_{O_2} v_s \left(P_{\mathrm{blood}} - \tilde{P}_{aO_2}\right) \tag{14}$$

with $Z_0 = 9.93$ mol.m^{-3} [1] is the haemoglobin concentration, $v_s = 1$ mm.s^{-1} [1] the mean blood velocity in the pulmonary capillary f the Hill's equation [55], i.e. $f(x) = x^{2.6}/(x^{2.6} + 26^{2.6})$ that gives the haemoglobin saturation versus the oxygen partial pressure in blood and $\sigma_{\mathrm{O_2,H_2O}}$ the solubility coefficient of oxygen in water. The quantity $\tilde{P}_{aO_2}) = 88$ mmHg is an effective partial pressure of oxygen in arterial pulmonary blood that accounts for potential previous visits of lung's alveoli by the blood. The value 88 mmHg is derived in order to get the correct quantity of oxygen flow to blood in the healthy case, see more details in [30]. The value of P_{blood} is computed by solving the non-linear equation (14) with a Newton method in Julia.

C- Numerical simulations

The algorithm for solving the model is implemented in the software Julia [50]. It is decomposed into two algorithms that are run successively: the first one computes the propagation of the infection; the second one computes the oxygen transport based on the output of the first one. Notice that the maximal generation of propagation for the infection (9 in this work) can be easily adjusted in our algorithm, as it is encoded using an integer variable. The computation time of an infection that reaches all the airways of the nine first generations is about 1 hour using a single core of a M1 processor.

Infection propagation.
The algorithm computing the infection propagation is decomposed into several steps:

1. Solve the infection equations independently of the airways for the whole duration of the disease. The dynamics of the infection is assumed to be the same in all the infected airways. What differs between the airways is the starting time of the infection.

2. Time $t = 0$. Define the initial infected airways list. In our model, the initial infected airways list consists in a single airway, the first in the fourth generation, i.e. index (4,1).

3. Time $t + dt$. For all the infected airways in the infected airways list, make the infection dynamics progress in each airway over a time step dt, according to the solution computed in step 2.

4. For all the infected airways in the infected airways list, test whether the neighbors of the airway are infected or not, depending on the number of pathogens in the corresponding infected airway. The probability of infection is determined using the function represented on Figure 5.

5. Add all the new infected airways to the infected airways list. The initial number of pathogens is equal to 500 for Cured cases, 850 for Aseptic death cases or 1200 for Septic death cases.

6. While the time is smaller than the maximum time of the infection, loop to step 3.

The output of the algorithm is a list of the index of the infected airways and of their degree of inflammation (variable Z) for each time step.

Oxygen transport.
The algorithm for the oxygen transport determines how oxygen is transported for each time step of the propagation of the infection. Since the infection propagates far slower than a ventilation cycle, the oxygen transport is determined for a typical ventilation cycle, i.e. assuming that the infection is quasi-static in time. However, the inflammation degree induces that the infected airways have a smaller radius, according to equation 11. As for oxygen transport, each time step is independent to the others, we can solve the time steps independently in parallel, using multiprocessing. The algorithm for oxygen transport is decomposed into several steps. Given a time step of the infection dynamics:

1. Compute the radii of the airways using the inflammation data computed by the infection algorithm. From the radii, the hydrodynamic resistance $R_{i,j}$ of each airway is computed.

2. Compute the equivalent hydrodynamic resistance $R^{eq}_{i,j}$ of the subtrees spanning from each airway. These resistances are computed going from the leaves of the tree towards the root of the tree.

3. Compute the path types: a path links one of the smallest airways to the largest airway of the tree. Two paths are of the same type if the deepest infected airways on the two paths are the same airway.

4. Compute the oxygen transport using the path types computed. The oxygen transport is solved using a normalized version of the equation (3) on each path types.

5. The solution is then reconstructed for the whole tree by assembling the solutions on each path types."